11-20-2017

Tip-enhanced Raman spectroscopy of amyloid β at neuronal spines.

Mohammadali Tabatabaei

Fabiana A Caetano

Farshid Pashee

Stephen S G Ferguson

François Lagugné-Labarthet

Analyst

ARTICLE

Tip-Enhanced Raman Spectroscopy of Amyloid β at Neuronal Spines

Received 00th January 20xx,
Accepted 00th January 20xx

DOI: 10.1039/x0xx00000x

www.rsc.org/

Mohammadali Tabatabaei,[a] Fabiana A. Caetano,[b] Farshid Pashee,[a] Stephen S. G. Ferguson,[c] François Lagugné-Labarthet.[a,†]

The early stages of Alzheimer's disease pathogenesis are thought to occur at the synapse level, since synapse loss can be directly correlated with memory dysfunction. Considerable evidence suggested that amyloid beta (Aβ), a secreted proteolytic derivative of amyloid precursor protein appears to be a critical factor in the early 'synaptic failure' that is observed in Alzheimer's disease pathogenesis. The identification of Aβ at neuronal spines with high spatial resolution and high surface specificity would facilitate unraveling the intricate effect of Aβ on synapses loss and its effect on neighboring neuronal connections. Here, tip-enhanced Raman spectroscopy was used to map the presence of Aβ aggregations in the vicinity of the spines exposed to Aβ preformed in-vitro. Exposure to Aβ was of 1 and 6 hours. The intensity variation of selected vibrational modes of Aβ was mapped by TERS for different exposure times to Aβ. Of interest, we discuss the distinct contributions of the amide modes from Aβ that are enhanced by the TERS process and in particular the suppression of amide I mode in the context of recently reported observations in the literature.

Introduction

Amyloid cascade hypothesis has been introduced almost 20 years ago for Alzheimer's disease (AD) as one of the most complicated neurodegenerative dementia and public health problems. The small fragment of amyloid beta (Aβ) peptide aggregates to form oligomers and eventually the macroscopic plaques. This overtime leads to gradual accumulation of Aβ in the brain striking a neurodegenerative cascade. The synaptic dysfunction promoted by the Aβ oligomers and the accelerated formation of neurofibrillary tangles culminate in synaptic failure and neuronal death.[1-4] Since the mechanisms behind the pathogenesis and onset of AD have not been clearly revealed, there are some doubts about the current Aβ hypothesis based on obtained contradictory experimental results. For instance, two recent reports of human trials treatment have failed even after 80 weeks of anti-amyloid antibody therapy.[5, 6] In addition, there are reports of AD without the presence of Aβ plaques and *vice versa*. However, none of these experimental data can argue the neurotoxicity of Aβ and its involvement in AD.[1] As a result, Aβ should be still a pivotal part of any revised thinking on AD's pathophysiology. The concept of the present work study with regards to the Aβ hypothesis cascade has been illustrated in Scheme 1. A neuron consists of a nucleus that generates two types of cell bodies referred as dendritic and axonic projections. These projections generate smaller connections, so-called spines, to connect with the projections of other neurons. Spines have different types of morphologies. In most of the spines, there is a rounded head (the spine head), and a neck that connects the head of the spine to the shaft of the dendrite. Spines can be generated from both axonic and dendritic projections. When the dendritic spines meet with a single spine of an axon, it can create a synapse (or spine event) to create a connection with one another through neurotransmitters exchange.[7] As shown in scheme 1, in a healthy synapse, different chemicals such as neurotransmitters can easily be transferred between pre-synaptic and post-synaptic sites of neurons. With the accumulation of Aβ oligomers and eventual plaques formation and deposition, these plaques can block the receptors at the surface of spines impairing the neuronal communication. This miscommunication results in impaired signalling and eventually synaptic loss.

In this context, plasmon-mediated spectroscopic techniques such as tip-enhanced Raman spectroscopy (TERS) can play a pivotal role in probing the presence of synaptic inhibitors thus providing elements to validate the cascade hypothesis associated with AD. The spatially resolved spectral and topographical details provided by TERS together with an improved surface specificity are critical factors to probe the presence of Aβ located in the vicinity of spinal junctions with a

[a] Department of Chemistry and Centre for Advanced Materials and Biomaterials, University of Western Ontario, London, ON, Canada N6A 5B7.
[b] Department of Physiology and Pharmacology, University of Western Ontario, London, Ontario, Canada N6A 5C1.
[c] Department of Cellular and Molecular Medicine, University of Ottawa, Ottawa, ON, Canada K1H 8M5.
† Corresponding author. Email: flagugne@uwo.ca

Electronic Supplementary Information (ESI) available: TERS experimental procedure, conventional and GSD-super resolution fluorescence microscopies of hippocampal neurons; AFM morphologies of non-exposed neurons and confocal bulk Raman signature of extracellular Aβ plaques with their vibrational assignment. See DOI: 10.1039/x0xx00000x

spatial resolution that surpasses confocal microscopy.[8] Furthermore, TERS does not require any labelling agent and is sensitive not only to the molecular structure, but also to the conformation of complex molecules forming biologically relevant polymorphs.

Aβ has been the subject of TERS studies for tracking the structural variations on a single insulin fibril,[9] to evaluate the nanoscale heterogeneity of individual amyloid fibrils polymorphs[10] as well as to discriminate toxic oligomers with ~30 nm spatial resolution.[11] In addition to TERS, surface-enhanced Raman spectroscopy (SERS) has been exploited for Aβ detection using nanoshells and nanofluidics.[12, 13] These individual pieces of information are very valuable to critically assess surface chemistry from different types of extracellular Aβ aggregations, albeit they have not yet been applied to probe the presence of Aβ aggregation in the vicinity of cellular structures.

Herein, TERS experiments were conducted on neuronal spines exposed to Aβ treatment. Chemical mapping of Aβ aggregates was specifically conducted in the vicinity of the projections of neurons thus benefitting, label-free, surface sensitivity and specificity, along with better spatial resolution enabled by TERS. It has been observed that the Aβ proteins forming the plaques show distinctive Raman spectral features. Aside from these spectral variations, the Aβ plaques located at neuronal spines have been observed by TERS after treatment with the preformed oligomers of Aβ for durations of 1 and 6 hours.

Experimental

Materials. Plastic dishes (35 mm) with glass bottoms (thickness of 0.16-0.19 mm) were purchased from MatTek Corporation. $A\beta_{1-42}$ peptide was purchased from American Peptide Co. (Sunnyvale, CA) with the sequence of NAEFRHNSGYEVHHQKLVFFAENVGSNKGAIIGLMVGGVVIA.

Culture of neuronal cells. Primary hippocampal mice neurons were dissociated in Hank's balanced salt solution (HBSS) and plated in NeurobasalTM medium supplemented with 0.5 mM L- glutamine, 2% B27 and 0.8% N2 supplements, and 50 units.mL^{-1} penicillin-streptomycin (Invitrogen). Cultures were then plated onto the glass coverslips at a density of 1×10^6 cells/dish. The cultures were incubated at 37°C for 21 days. The medium was also changed every 2-3 days. Animal handling protocol was in accordance with Western University (The University of Western Ontario) Animal Care Committee.

Aβ preparation for neuronal cultures. $A\beta_{1-42}$ peptides were suspended in an F12 medium (no phenol red) followed by sonication. They were let sit for at least 24 hours in the fridge (4°C) to form the oligomers. They were then kept at -80°C. These peptides were found to occur in a predominantly oligomeric form which was more toxic to hippocampal neurons than the fibrillar form. The prepared Aβ oligomer solutions were thermally equilibrated to ambient temperature before injecting into living neuronal cultures. Neuronal cultures (at the density of 1×10^6 cells/dish) were then treated with 10 µL of 1 µM of Aβ oligomers, in HBSS buffer, for 1 or 6 hours and incubated at physiological conditions with 37°C temperature. Cells were then fixed using a solution of 4% paraformaldehyde and 4% sucrose prepared in phosphate buffered saline (PBS, pH 7.4, Invitrogen) for 20 minutes at room temperature.

TERS setup. The TERS setup and tip preparation are detailed in the supporting information section and Figure S1.

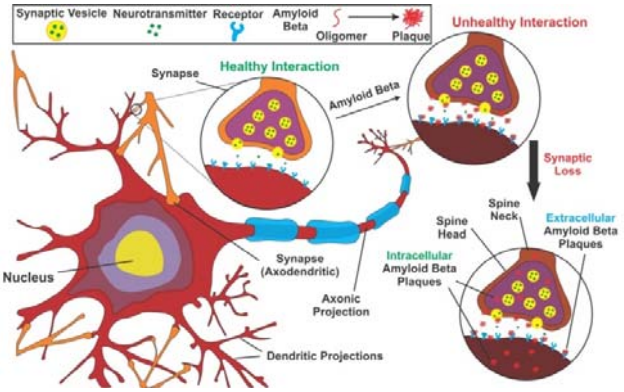

Scheme 1. The synopsis concept of amyloid cascade hypothesis

Results and discussion

Proteins located at spine sites can be precisely probed by a TERS tip to benefit from plasmon-mediated local enhancement of the excitation field at the apex of the metallic tip. This confined enhancement, therefore, enables a high spatial resolution of the optical measurements that surpasses confocal microscopy measurements. TERS is a surface specific technique due to the very limited spatial extension of the tip-enhanced signal. This yields to measurements which are predominantly sensitive to the extracellular Aβ plaques located on the surface of the spines. This critical aspect will be further discussed in this manuscript.

Morphological information of neuronal connections. As shown in Fig. S2A, visualizing the spines in a neuronal projection is not readily obtainable using conventional epi-fluorescence wide-field imaging. Other advanced optical microscopic techniques such as ground-state depletion (GSD) or stimulated emission depletion (STED) super-resolution fluorescence imaging can facilitate the imaging of smaller and poorly-contrasted features.[14-17] Shown in Fig. S2B, GSD super-resolution fluorescence offers better resolution beyond the diffraction limit to observe the localization of spines at neuronal projections. However, even these techniques are limited to the spatial resolution of ~20 nm and yet need labelling of the sample which is often incompatible with in-vitro studies due to the toxicity of the fluorophores used.

In the context of bio-imaging developments, AFM can provide spatial resolutions better than 1 nm under a variety of biologically compatible conditions (controlled temperature or fluid conditions). Herein, AFM was first employed on fixed cells in order to obtain detailed nanoscale morphological conformations of the neurons with their projections and spines. AFM topography images were obtained from non-

treated neurons (Fig. S3) and neurons exposed 1 hour to Aβ (Fig. 1). In Fig. 1 and Fig. S3, a nucleus of a neuron with its main projections can be identified. The other projections of the neuron with its spines are shown in Fig. 1B-D. The localization of spines on the selected regions of the projection is highlighted in Figs. 1C,D as well as in Fig. S3. As shown in Fig. 1C, the isolated spine is found to be ~1 µm long. This is in good agreement with the morphology that has been observed for live mouse cortical neurons.[14, 18]

AFM scans of reference Aβ structures grown on freshly cleaved mica were conducted separately to identify aggregates of oligomers and plaque formation (Fig. S4). The variation of morphologies of these plaques is highlighted by Aβ plaques with different diameters from ~130-570 nm and ~ 9-55 nm thicknesses as evidenced by the AFM cross sections (Fig. 2B,C). Confocal Raman spectra were collected on the same sample showing a uniform signature independently of the aggregate dimension (Fig. S5 and Table S1). The spectra and vibrational assignment of Aβ plaques can be used as a basis for the comparison with the TERS signals of the Aβ proteins at neuronal spines. Importantly, when grown in the presence of Aβ, the morphology of the spines can be affected.[19] Thus, beyond the pure spatial resolution and surface specificity, TERS enables the direct correlation between surface morphology and molecular information though the analysis of the collected spectra. It is, however, important to recall that tip-enhanced spectra do not necessarily exhibit identical spectral features as compared to confocal Raman signal. This can be due to a variety of factors including polarization and molecular orientation as well as gradient-field effects that can be critical in TERS experiments.[20-22] It has also been reported that TERS spectra from proteins such as amyloid, collagen and insulin fibrils, could differ significantly from laboratory to laboratory and even within the same experimental series.[23, 24]

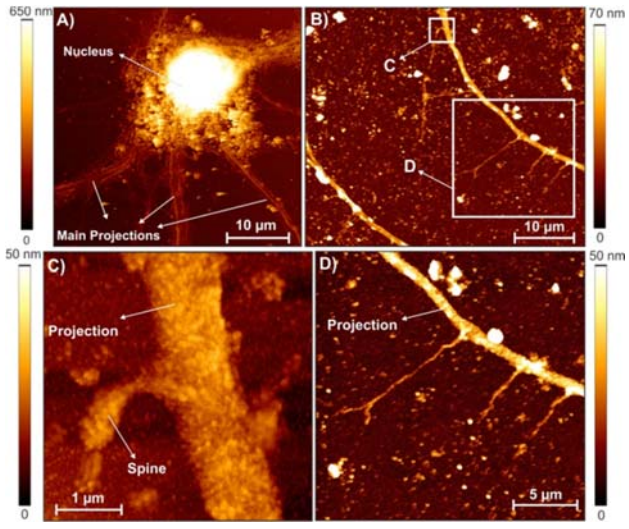

Figure 1. Nanoscale morphology of neuronal projections and spines exposed 1 hour to Aβ. A) AFM morphology of a neuronal nucleus and projections. B) AFM morphology of neuronal projections and spines. C-D) selected regions on B, demonstrating the localization of projected spines out of the projections.

TERS mapping of Aβ plaques at neuronal spines. Subsequent to the individual morphological information of the projections and Aβ, TERS spectra were collected and analysed to map the Aβ distribution at neuronal spines (Fig. 2). Neurons without any treatment of Aβ oligomers have been used as control samples and a representative TERS spectrum is labelled as (1) in Fig. 2A. Typical TERS spectra obtained on neurons treated for 1 h with Aβ prior to fixation are labelled as (2) and (3) in Fig. 2A. Confocal Raman spectra with no TERS tip yielded no exploitable signal even with longer acquisition time or more intense laser excitation. This is presumably due to the small thickness and lateral dimensions of the spine membrane. The suppression of amide I peak has been observed in most of the collected spectra and statistical measurements are provided in a later section of this manuscript. However, some tip-enhanced Raman spectra of the Aβ plaque show the amide I peak on the treated neurons and are labelled as (3) in Fig. 2A.

Mapping was performed over a selected spine treated with Aβ by step scanning the TERS tip over an area composed of 19x23 points with an acquisition time of 5 s per spectrum. The resulting 437 spectra were acquired in about 40 minutes. A step scan resolution of 100 nm was used in order to minimize collection time and associated instrumental drift. Considering the size of the spines of several hundred nm, this selected spatial resolution was well adapted for this study. The true TERS resolution is limited to the TERS tip diameter and is estimated to be around ~30 nm (Fig. S1). Nevertheless, spatial resolution better than the tip diameter could be reached if small metallic particles are located at the extremity of the tip. Five spectral regions were selected to map out the spatial distribution of vibrational modes over treated spines. The region of 2850-3000 cm^{-1} was used show the C-H modes associated mostly with the membrane-containing lipids and minimaly with the C-H modes of the Aβ protein since no major change of intensity was observed in this spectral range across the spines as shown in spectra noted (1) and (2) in Fig. 2A.[25] Due to minimal spectral overlaps with non-treated neurons in the 1200-1300 cm^{-1} region, the C-C ring breathing (1200-1230 cm^{-1}), amide III disordered (1235-1260 cm^{-1}), amide III α-helix (1265-1295 cm^{-1}) were selected to be mapped. The C-C breathing modes come from the amino acids of the Aβ that contains aromatic cycles (Phe and Tyr). The amide I mode (1655-1675 cm^{-1}) was also a probe of interest. By integrating the TERS intensity of the selected modes, five maps representing the spatial distribution of these modes were generated (Fig. 2B) and overlaid with the AFM morphology of a selected spine as shown in Fig. 2C. Fig.2 is completed by Fig.S6 showing the TERS spectra with common scale of the background (glass coverslip) together with regions rich and poor in Aβ aggregates.

The amide III disordered mode has the most distinct mapping on the spine showing a heterogeneous accumulation of Aβ. This distribution of collected spectra suggests that the exact structure (or a mixture of structures) of the Aβ varies in these specific areas of spines and are dependent on the conformational changes of the proteins. The spectral shifts in the amide III region are indicators of structural changes in

proteins and are used to quantitatively explore secondary structures.[13] This distribution clearly suggests that the exact structure of the Aβ varies in these specific areas of spines and it is mostly dependent on the conformational changes of the protein. It is known that Raman spectroscopy provides a wealth of information on the change of their secondary structure during protein aggregation and amyloid fibril formation and is sensitive to concentration and pH as highlighted in resonance Raman, SERS and TERS experiments.[10, 26, 27] In particular, the amide III mode in the 1200-1300 spectral range provides compelling spectral changes that can be exploited to analyse secondary structures.[13] As such, a tentative assignment reveals that the Aβ is mostly observed in the disordered Aβ (1254 cm^{-1}) plaques form compared to Aβ that displays α-helix (1270 cm^{-1}-amide III) and β-sheet (1240-1244 cm^{-1}-amide III) based on SERS measurements done on Aβ oligomers[13] or single amyloid fibril measurements.[9]

After treatment of neurons with Aβ oligomers, Aβ plaques are presumably either fully internalized into the neuronal membrane and/or exist at the surface of the spines and bound to a receptor. At this stage, it is important to discuss the sensitivity of TERS for the detection of internalized Aβ plaques. As mentioned earlier, since the axial extension of the plasmon-mediated TERS effect is limited to a few nanometers, TERS is known to be a surface-sensitive spectroscopy. In these conditions, one may examine the potential of TERS to probe internalized Aβ plaques. Here, one has to first consider the 5 nm thickness of the neuronal membrane[28] that the plasmon-mediated surface enhancement must surpass at both excitation and collection events. Due to this very small thickness of the spine membrane, it is likely possible that the TERS tip would sense both cases of fully internalized amyloid beta proteins and the ones that are bound externally to the receptors at the membrane. However, Aβ is a weak scatterer and the extension of the TERS effect is known to be a near-field effect that vanishes by 90 % within the first 20 nm.[21]

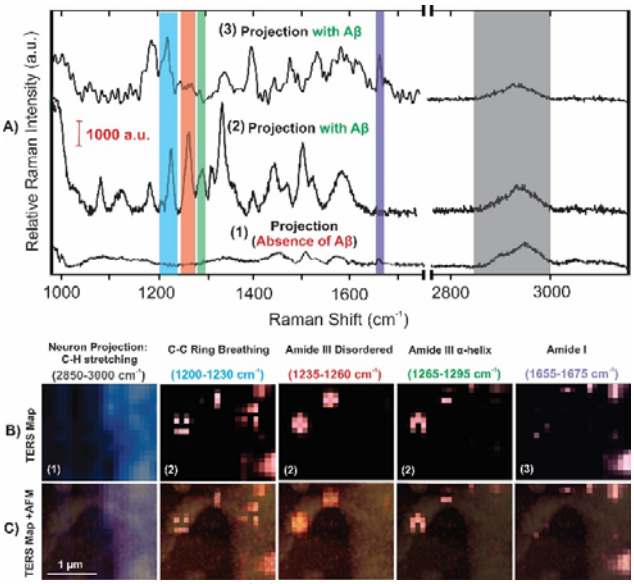

Figure 2. TERS spectra and maps of Aβ at neuronal spines with representative signals. A) TERS spectra of non-treated (1) and treated (2,3) neuronal projections with Aβ. B) TERS maps with different spectral integrated regions as stated. C) The overlap of the TERS maps with the AFM morphology of a spine shown in Fig. 3C.

It is, therefore, less likely to probe the completely internalized Aβ that has passed the membrane and the TERS experiments will be more significantly sensitive to the amyloid beta bound to the membrane receptors located at the spine surface. This analysis goes beyond the scope of the present work and it would be indeed of critical interest to evaluate and calibrate TERS sensitivity towards buried molecules. Here our measurements are mostly sensitive to Aβ bound to protein receptors located in the spine membrane.

Variations and statistics of TERS signals of Aβ plaques at spines. A collection of representative TERS spectra of Aβ signal collected from distinct 100 spines projected from 10 neuronal projections treated with Aβ oligomers for 1 hour is shown in Fig. 3.

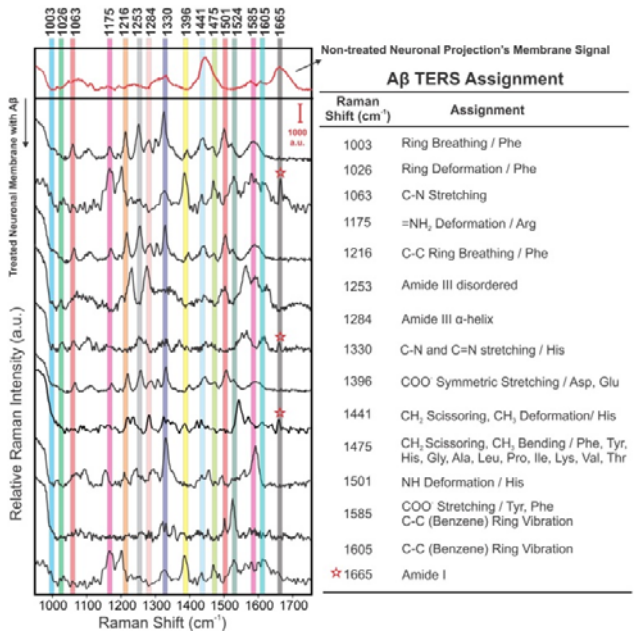

Figure 3. TERS spectra of Aβ and spectral assignment.[9, 13, 23, 29-31] Amide I suppression is observed in most spectra. The representative signal with Amide I mode is highlighted with a red star.

For sake of comparison, the TERS spectrum of a non-treated neuronal projection's spine membrane is shown in Fig. 3 as a reference. Similar variations between TERS signals of Aβ plaques have been shown in this figure with the corresponding vibrational assignment. Although there are some variations, this proves the sensitivity of TERS to small changes. Besides, as mentioned before, it is reported in the literature that TERS spectra from various amyloid structures could differ significantly even within the same experimental series.[23] As shown in Fig. 3, the amide I peak is missing in the majority of the collected spectra, however, some areas of the sample have shown this peak in their signal as shown in this figure (red star). Missing amide I peak has been reported in a variety of specimens, either fully or partially, in several SERS,[32, 33] and TERS [10, 23, 27, 31, 33] studies. There are several suggestions to account for these observations including strong interaction of backbone with metal (Au, Ag), random orientation of the protein with respect to the tip and excitation laser polarization's longitudinal and lateral components, different selection rules between Raman and TERS, and shielding of the protein backbone by the amino acid side chain.[23, 33] It has also been reported for TERS studies that the lack of signal to noise ratio due to the dominant peaks of the benzene C-C ring vibration at 1585 and 1605 cm^{-1} could also play a role.[31] In the case of SERS-based label-free measurements, the major challenge is the poor reproducibility causing some spectra to show amide I while the rest lack the signal.[32] Reproducibility is extremely important in such measurements. Spectra with suppressed amide I band are observed more frequently in SERS with silver nanoparticles than with gold.[33]

Effect of Aβ exposure time to the neurons on TERS signals. The effect of Aβ oligomers exposure time to the neurons on the resulting TERS signal was evaluated (Figure 4). We used the statistical analysis to represent the intensity variations of the same selected peaks in the mapping and also the percentage of their presence at spines depending on the exposure time scales. The TERS control sample is the neurons without any Aβ exposure. These results were obtained from the statistical analysis of 100 spines from ~10 neurons in each of three types of samples including neurons without any exposure and also Aβ exposure time scales of 1 and 6 hours prior to the measurements.

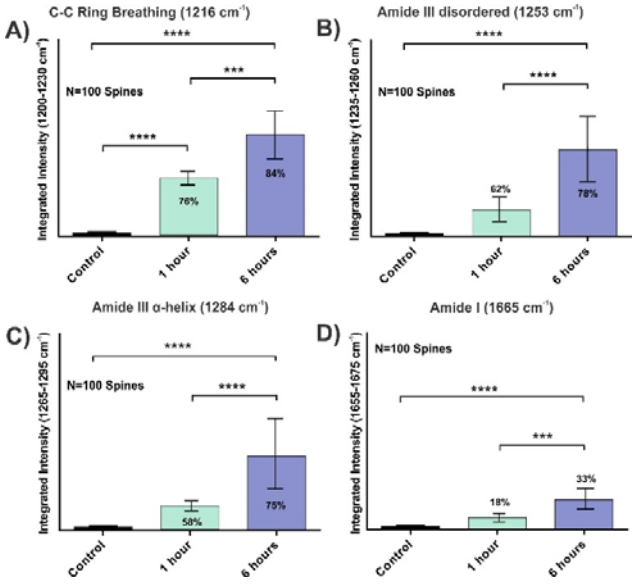

Figure 4. Aβ TERS signals comparison of 100 spines for different Aβ exposure time scales with different integrated areas including A) C-C Ring breathing; B) Amide III disordered; C) Amide III α-Helix; D) Amide I β-Sheet. The spines of neurons without any exposure to Aβ oligomers are selected as control. The percentages for 1 and 6 hours Aβ exposure represent the number of spines generating signals higher than the control signal. Mean values have been used for integrated intensities. Error bars represent the standard deviations. Tukey multiple comparison test with 95% confidence interval was used to test the significance of the difference. [**** $p < 0.0001$; *** $p < 0.001$]

As shown in Figure 4, the intensity of Aβ signals after 6 hours of treatment is significantly higher than after only 1 hour. This is definitely related to the accumulation rate after 1 hour due to the probable extreme low concentration of Aβ at spines. The probability of finding neurons with signals of Aβ after 1 and 6 hours of treatment vary depending on the selected region of integration. According to the amide III disordered peak, the signal was observed for 62% and 78% of the spines after 1 and 6 hours of Aβ exposure, respectively. However, this is different for C-C ring breathing, amide III α-helix and amide I peaks as shown in Fig. 6. Although, they all showed the same trend between control as well as 1 and 6 hours of exposure time scales. Exceeding 6 hours of treatment would significantly increase the possibility of neuronal death, which interferes with the purpose of the study. Noteworthy, the probability of finding the amide I peak after 1 and 6 hours of Aβ exposure was 18% and 33%, respectively. This suggests that

the amide I peak was missing in more than 77% of the areas where the TERS signal was collected. Regarding the local signal enhancement provided by the TERS measurement, since no signal was observed in confocal mode (tip out), we were not able to experimentally determine an enhancement factor from these precise biological samples. Importantly, TERS measurements provide surface sensitivity that can be exploited to study complex mechanisms at surfaces and interfaces.

Conclusion

In this explorative work, we have imaged neuronal spines treated with Amyloid β using Tip-enhanced Raman spectroscopy. We are not only demonstrating the variety of spinal morphologies with AFM but also revealing, for the first time, the heterogeneous Aβ accumulations at the surface of spines using label-free TERS measurements. TERS maps suggested a Aβ accumulation based on the amide III disordered region, perhaps mostly in the forms of plaques, in different regions of spines specifically at the neck and head of spines. We have also observed the variations not only between confocal Raman and TERS signals but also within same TERS signals collected at different spines. The spectral information suggested the amide I peak suppression in more than 77% of the collected spectra that can be attributed to different reasons including the shielding of the protein backbone by amino acid side chains, the orientation of the proteins with respect to the TERS probe. It was also observed that both exposure time periods of 1 and 6 hours of Aβ oligomers to the neurons introduced the presence of Aβ with a significant formation of plaques after 6 hours compared to 1 hour. This opens up a new opportunity in this field to use TERS as a tool to facilitate the process of unveiling the mechanism at work behind the role of Aβ in AD. This study can be pursued further by applying TERS to more controlled systems by combining it with cell micropatterning.[25, 34-36] This line of research can also be explored by studying the neurons at different phases of AD and the effect of Aβ inhibitors at molecular level towards a better understanding of the mechanism at work behind AD.

Acknowledgements

The authors gratefully acknowledge the Nanofabrication (tip coating) and the Confocal Microscopy (GSD) Facilities at the University of Western Ontario. This research was funded by the Canada Research Chairs programs in “Photonics and Nanosciences” (F. L.-L.) and “Molecular Neurobiology” (S. S. G. F.) as well as the NSERC Discovery Grant program (F. L. -L.).

Notes and references

1 K. Herrup, *Nat. Neurosci.*, 2015, 794-799.
2 Tara L. Spires-Jones and Bradley T. Hyman, *Neuron*, 2014, **82**, 756-771.
3 J. J. Palop and L. Mucke, *Nat. Neurosci.*, 2010, **13**, 812-818.
4 L. Bertram, C. M. Lill and R. E. Tanzi, *Neuron*, 2010, **68**, 270-281.
5 R. S. Doody, R. G. Thomas, M. Farlow, T. Iwatsubo, B. Vellas, S. Joffe, K. Kieburtz, R. Raman, X. Sun, P. S. Aisen, E. Siemers, H. Liu-Seifert and R. Mohs, *N. Engl. J. Med.*, 2014, **370**, 311-321.
6 S. Salloway , R. Sperling , N. C. Fox , K. Blennow , W. Klunk , M. Raskind , M. Sabbagh , L. S. Honig , A. P. Porsteinsson , S. Ferris , M. Reichert , N. Ketter , B. Nejadnik , V. Guenzler , M. Miloslavsky , D. Wang , Y. Lu , J. Lull , I. C. Tudor , E. Liu , M. Grundman , E. Yuen , R. Black and H. R. Brashear *N. Engl. J. Med.*, 2014, **370**, 322-333.
7 I. M. Ethell and E. B. Pasquale, *Prog Neurobiol.*, 2005, **75**, 161-205.
8 F. Pashaee, M. Tabatabaei, F. A. Caetano, S. S. G. Ferguson and F. Lagugné-Labarthet, *Analyst*, 2016, **141**, 3251-3258.
9 T. Deckert-Gaudig, E. Kämmer and V. Deckert, *J. Biophotonics*, 2012, **5**, 215-219.
10 C. C. vandenAkker, T. Deckert-Gaudig, M. Schleeger, K. P. Velikov, V. Deckert, M. Bonn and G. H. Koenderink, *Small*, 2015, **11**, 4131-4139.
11 S. Bonhommeau, D. Talaga, J. Hunel, C. Cullin and S. Lecomte, *Angew. Chem. Int. Ed.*, 2017, **56**, 1771-1774.
12 H. T. Beier, C. B. Cowan, I.-H. Chou, J. Pallikal, J. E. Henry, M. E. Benford, J. B. Jackson, T. A. Good and G. L. Coté, *Plasmonics*, 2007, **2**, 55-64.
13 I. H. Chou, M. Benford, H. T. Beier, G. L. Coté, M. Wang, N. Jing, J. Kameoka and T. A. Good, *Nano Lett.*, 2008, **8**, 1729-1735.
14 S. Berning, K. I. Willig, H. Steffens, P. Dibaj and S. W. Hell, *Science*, 2012, **335**, 551-551.
15 U. V. Nägerl, K. I. Willig, B. Hein, S. W. Hell and T. Bonhoeffer, *Proc. Natl. Acad. Sci. USA*, 2008, **105**, 18982-18987.
16 P. Monaghan, D. Green, J. Pallister, R. Klein, J. White, C. Williams, P. McMillan, L. Tilley, M. Lampe, P. Hawes and L.-F. Wang, *Virol. J.*, 2014, **11**, 1-12.
17 J. Folling, M. Bossi, H. Bock, R. Medda, C. A. Wurm, B. Hein, S. Jakobs, C. Eggeling and S. W. Hell, *Nat. Meth.*, 2008, **5**, 943-945.
18 M. Maglione and S. J. Sigrist, *Nat. Neurosci*, 2013, **16**, 790-797.
19 P. N. Lacor, M. C. Buniel, P. W. Furlow, A. Sanz Clemente, P. T. Velasco, M. Wood, K. L. Viola and W. L. Klein, *J. Neurosci.*, 2007, **27**, 796-807.
20 L. Billot, M. Lamy de la Chapelle, A.-S. Grimault, A. Vial, D. Barchiesi, J.-L. Bijeon, P.-M. Adam and P. Royer, *Chem. Phys. lett.*, 2006, **422**, 303-307.
21 C. C. Neacsu, S. Berweger and M. B. Rashke, *Nanobiotechnology*, 2009, **3**, 172-196.
22 E. J. Ayars, H. D. Hallen and C. L. Jahncke, *Phys. Rev. Lett.*, 2000, **85**, 4180-4183.
23 M. Paulite, C. Blum, T. Schmid, L. Opilik, K. Eyer, G. C. Walker and R. Zenobi, *ACS Nano*, 2013, **7**, 911-920.

24 C. Blum, L. Opilik, J. M. Atkin, K. Braun, S. B. Kämmer, V. Kravtsov, N. Kumar, S. Lemeshko, J.-F. Li, K. Luszcz, T. Maleki, A. J. Meixner, S. Minne, M. B. Raschke, B. Ren, J. Rogalski, D. Roy, B. Stephanidis, X. Wang, D. Zhang, J.-H. Zhong and R. Zenobi, *J. Raman Spectrosc.*, 2014, **45**, 22-31.

25 M. Tabatabaei, G. Q. Wallace, F. A. Caetano, E. R. Gillies, S. S. G. Ferguson and F. Lagugné-Labarthet, *Chem. Sci.*, 2016, **7**, 575-582.

26 D. Kurouski, R. A. Lombardi, R. K. Dukor, I. K. Lednev and L. A. Nafie, *Chem Commun.*, 2010, **46**, 7154-7156.

27 D. Kurouski, R. P. Van Duyne and I. K. Lednev, *Analyst*, 2015, **140**, 4967-4980.

28 S. M. Breedlove and N. V. Watson, *Biological Psychology: An Introduction to Behavioral, Cognitive, and Clinical Neuroscience.* , Sinauer Associates Inc., Seventh edn., 2013.

29 J. Dong, C. S. Atwood, V. E. Anderson, S. L. Siedlak, M. A. Smith, G. Perry and P. R. Carey, *Biochemistry*, 2003, **42**, 2768-2773.

30 T. Demeritte, B. P. Viraka Nellore, R. Kanchanapally, S. S. Sinha, A. Pramanik, S. R. Chavva and P. C. Ray, *ACS Appl. Mater. Interfaces*, 2015, **7**, 13693-13700.

31 C. Blum, T. Schmid, L. Opilik, N. Metanis, S. Weidmann and R. Zenobi, *J. Phys. Chem. C*, 2012, **116**, 23061-23066.

32 L.-J. Xu, C. Zong, X.-S. Zheng, P. Hu, J.-M. Feng and B. Ren, *Anal. Chem.*, 2014, **86**, 2238-2245.

33 D. Kurouski, T. Postiglione, T. Deckert-Gaudig, V. Deckert and I. K. Lednev, *Analyst*, 2013, **138**, 1665-1673.

34 M. Tabatabaei, F. A. Caetano, S. Vedraine, P. R. Norton, S. S. G. Ferguson and F. Lagugné-Labarthet, *Biomaterials*, 2013, **34**, 10065-10074.

35 A. Leclair, S. S. G. Ferguson and F. Lagugné-Labarthet, *Biomaterials*, 2011, **32**, 1351-1360.

36 S. Varma, J. McLachlan, A. Leclair, B. C. Galarreta, P. R. Norton and F. Lagugné-Labarthet, *Anal. Bioanal. Chem.*, 2010, **396**, 1159-1165.

37